Transactions on Electrical and Electronic Materials (2019) 20:522–529
https://doi.org/10.1007/s42341-019-00144-4

Online ISSN 2092-7592
Print ISSN 1229-7607

REGULAR PAPER

Fabrication of Bismuth Vanadate ($BiVO_4$) Nanoparticles by a Facile Route

M. F. Rahman[1] · M. S. Haque[1] · M. Hasan[1,2] · M. A. Hakim[1]

Received: 18 May 2019 / Revised: 3 September 2019 / Accepted: 12 September 2019 / Published online: 17 September 2019

Abstract

Monoclinic bismuth vanadate (m-$BiVO_4$) has attracted many researchers as an advanced photocatalyst for hydrogen production via water splitting and degradation of organic contaminants. In this study, pure m-$BiVO_4$ nanoparticles were fabricated by an easy reproducible solid state route at different temperatures (500 °C, 550 °C, 600 °C, 650 °C and 700 °C) for 2 h. The synthesized materials were characterized by X-ray Diffractometer where all the diffraction patterns reveal characteristic peaks corresponding to m-$BiVO_4$ with space group C2/c. Obtained m-$BiVO_4$ particles have the lattice parameters: a = 7.2477 Å, b = 11.6970 Å, c = 5.0900 Å and the volume of the unit cell is 309.23 (10^6 pm^3). Fourier Transform Infrared spectroscopy exhibits formation of Bi–O bond in the prepared nano powders. Ultraviolet–Visible diffuse reflectance spectroscopy suggests that nanostructured $BiVO_4$ particles possess strong energy absorption properties both in visible and ultraviolet region. The particles show red shift of band gap as the calcination temperature rises and possible reasons have been discussed. Energy-dispersive X-ray spectroscopy confirms presence of Bi, V, and O without any contaminant, while particle's morphology was investigated using Field Emission Scanning Electron Microscope.

Keywords Monoclinic bismuth vanadate · Solid state reaction · Nanoparticles · Lattice strains

1 Introduction

The hydrosphere is getting polluted because of high population growth and rapidly growing industrialization. On the contrary, the demand of pure water is soaring both for industrial and domestic use. Consequently, purification of contaminated water through a low cost green sustainable technique has emerged as a crucial issue. Another cardinal challenge is to meet the rising energy need which is now mostly dependent on fossil fuels. As fossil fuels are deleterious to environment, generation of hydrogen energy through utilization of solar energy is being reckoned as potential green energy source. So, it is high time to develop new semiconductor materials which can exploit solar energy by converting it into electrical and chemical energy [1–4]. Semiconductor photocatalysts have emerged as promising materials for water splitting and degradations of organic contaminants [5]. However, the performance of the photocatalyst material relies on several factors such as crystal structure, morphology and synthesis route [6]. Though various metal oxides like TiO_2 [7, 8], SnO_2 [9], ZnO [10, 11], Cu_2O [12, 13], Ag_3VO_4 [14], $InVO_4$ [14], $BiVO_4$ [15] have been formulated to date, $BiVO_4$ has drawn great attention to the scientific community owing to its unique properties like non-toxic nature, low band gap energy [16–20]. $BiVO_4$ occurs naturally as the mineral pucherite with an orthorhombic crystal structure while synthetic $BiVO_4$ has mainly three crystalline phases: tetragonal zircon, monoclinic scheelite and tetragonal scheelite [21, 22]. Monoclinic scheelite structure has been found to be the most suitable photocatalyst among the crystals of $BiVO_4$ because of having narrow band gap (2.4 eV) [23–25]. The crystal system of m-$BiVO_4$ has four unique lattice sites: Bi (4e), V (4e), O_1 (8f), and O_2 (8f) where O_1 is aligned with one Bi and V, whereas O_2 is aligned with 2 Bi and a single V [26]. This system possesses

M. F. Rahman and M. S. Haque have contributed equally to the work.

✉ M. F. Rahman
farabigce@gce.buet.ac.bd

[1] Department of Glass and Ceramic Engineering, Bangladesh University of Engineering and Technology, Dhaka 1000, Bangladesh

[2] Department of Materials Science and Engineering, North Carolina State University, Raleigh, NC 27606, USA

oxidation states of 3^+, 5^+ and 2^- for Bi ($5d^{10}$ $6s^2$), V ($3d^0$) and O ($2p^6$) respectively and crystal distortion present in monoclinic phase increases lone pair effect of Bi 6*s* states resulting O 2*p* states moving upwards [27]. Consequently, band gap reduces to 2.4 eV in monoclinic phase compared to 2.9 eV in tetragonal phase which enables electronic transition by visible light from occupied O 2*p* states to the unoccupied V 3*d* states [27]. Furthermore, separation efficiency of photo induced electrons and holes is higher in m-$BiVO_4$ due to distortion in Bi-O bond [27]. In this perspective, various methods have been employed for the preparation of m-$BiVO_4$ nanoparticles such as hydrothermal process, molten salt method, solvothermal process, ultrasonic-assisted method, flame spray, microwave synthesis, sol–gel, mechanochemical synthesis, hybrid organic–inorganic route and co-precipitation method [28–39].

In this report, a simple reproducible solid state reaction method was explored for the preparation of nanostructured pure m-$BiVO_4$ from Bi_2O_3 and V_2O_5 as precursors at different temperatures (500 °C, 550 °C, 600 °C, 650 °C and 700 °C) for two hours. This study presents in depth analysis on structural formation, vibrational properties, optical band gap and morphology of pure m-$BiVO_4$ particles obtained employing solid state route which should facilitate to carry out further research on nanostructured m-$BiVO_4$.

2 Materials and Methods

In order to prepare m-$BiVO_4$ nanoparticles, a facile solid state method was adopted where analytical grade bismuth oxide: Bi_2O_3 (99.9%, Inframat Advanced Materials) and vanadium pentoxide: V_2O_5 (99%, Loba Chemie) were used as precursors without any further purification. The precursors were mixed together at stoichiometric 1:1 (Bi:V) molar ratio by hand milling with mortar and pestle, followed by calcination at different temperatures (500 °C, 550 °C, 600 °C, 650 °C and 700 °C) for 2 h in a muffle furnace (model LT 15/11/C450, Nabertherm). Then the obtained particles were subjected to characterizations.

An X-Ray Diffractometer system (model Empyrean, PANalytical) with Cu target was used to determine the phases present and other structural information where High score plus data base and VESTA graphical interface software were used to analyze XRD data. FTIR spectra (model Spectrum Two, Perkin Elmer) were recorded in the wave number range 400–4000 cm^{-1} for observing bonding conformation of the synthesized powders. UV–Vis spectroscopy (model Lambda 1050, Perkin Elmer) was performed in diffuse reflection mode in an interval 200–800 nm in order to determine the absorption properties of the particles and the corresponding optical band gap. Morphology of the particles was examined by FESEM (model JSM 7600F, JEOL), while elemental compositions were determined using EDS coupled with FESEM.

3 Results and Discussion

Room temperature XRD analysis was performed for the $BiVO_4$ samples using Cu-Kα (λ = 1.541874 Å) radiation at 2θ values between 10° and 80° in order to estimate the crystalline parameters as a result of increasing synthesis temperature. Phase identifications have been carried out with high score plus database provided by PANalytical. As displayed in Fig. 1a, all the samples exhibit monoclinic clinobisvanite $BiVO_4$ with space group C2/c (ICSD reference pattern code: 98-010-0605). Moreover, all diffraction patterns show the characteristic peak splitting at about 2θ = 18.5° and 35° (Fig. 1b). The presence of these distinctive phenomena in the XRD patterns obtained for the synthesized samples confirm the formation of monoclinic phase [40, 41]. For monoclinic $BiVO_4$, the crystallographic parameters and atomic fractional coordinates of all atoms are listed in Table 1.

However, along with desired spectra, few extra peaks of unreacted precursors and intermediate phases become visible (Fig. 1a) for nanoparticles synthesized at 500 °C and 550 °C. It reveals that these lower temperatures are not sufficient to complete the reaction entirely. Moreover, quantitative analysis by reitveld refinement shows the presence of about 70% and 90% of monoclinic $BiVO_4$ phase for 500 °C and 550 °C respectively elucidating effect of synthesis temperature on reaction yield. At higher temperatures above 550 °C, no additional diffraction peak of any intermediate phase has been detected, indicating the formation of single phase (m-$BiVO_4$) structure.

From the crystal structure, it is evident that the unit cell of monoclinic $BiVO_4$ is composed of VO_4 tetrahedron and BiO_8 dodecahedron. As shown in Fig. 2, the Bi site is bordered by eight oxygen atoms to form BiO_8 dodecahedron and the V site by four oxygen atoms making a VO_4 tetrahedron. Though the BiO_8 dodecahedron shares edges with nearby BiO_8 dodecahedra, each VO_4 tetrahedron is separated and does not come into contact with the neighboring VO_4 tetrahedron. By sharing an apex oxygen atom, the isolated VO_4 tetrahedron is connected with BiO_8 dodecahedron. The existence of four types of Bi–O bond and two types of V–O bond (Table 1) state that both VO_4 tetrahedron and BiO_8 dodecahedron are distorted.

The average crystallite size (D) was calculated using Scherrer formula: $D = K\lambda/(\beta_{size}\cos\theta)$ where K is the crystal shape factor, λ is the wavelength of Cu-Kα radiation used, θ is the bragg angle. Lattice strain was determined from the tangent formula: Lattice strain $= \beta_{strain}/(4*\tan\theta)$. In the above two equations, β describes the structural broadening in radians which is the difference between integral profile width of

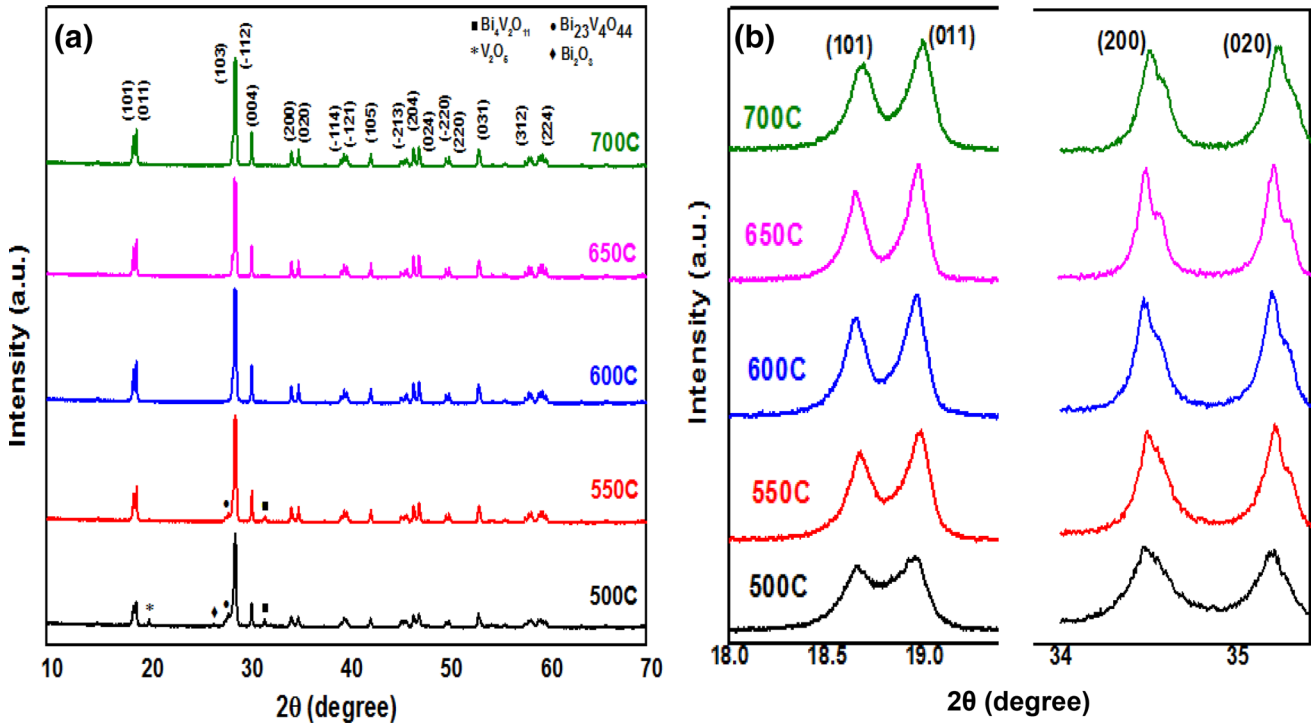

Fig. 1 **a** XRD patterns of synthesized $BiVO_4$ particles and **b** peak splitting of (101) and (200) planes for monoclinic $BiVO_4$ phase

Table 1 Crystallographic parameters, atomic positions and bond lengths between different atoms of monoclinic clinobisvanite $BiVO_4$

a (Å)	b (Å)	c (Å)	α = γ (°)	β (°)	Calculated density (g/cm^3)	Volume of the cell (10^6 pm^3)
Crystallographic parameters						
7.2477	11.6970	5.0900	90	134.2230	6.96	309.23
O1			O2		V1	Bi1
Atomic fractional coordinates						
(0.26060, 0.44930, 0.37960)			(0.14650,0.20820,0.13880)		(0,0.13000,0.25000)	(0,0.63350,0.25000)
Bi-O (Å)					V–O (Å)	
Bi1-O1			Bi1-O2		V1-O1	V1-O2
Bond lengths						
2.52526 × 2			2.34484 × 2		1.74303 × 2	1.74661 × 2
2.60470 × 2			2.37356 × 2			

standard and test sample: $\beta_{size} = \beta_{obs} - \beta_{std}$ and β_{strain} = Square root $(\beta^2_{obs} - \beta^2_{std})$

From Table 2, it is observed that crystallites become larger with increasing synthesis temperature which may be due to the crystallization process through accelerating the Bi^{3+} ions diffusive into VO_4^{3-} anions [42–44]. However, value of lattice strain varies inversely with temperature. The synthesized $BiVO_4$ at 700 °C shows lowest strain which validates the higher degree of crystallization of $BiVO_4$ at higher temperature [42]. In addition, a reverse relation exists between crystallite size and lattice strain resembling the previously reported work [3, 45–49]. Indeed, the grain boundaries of nanostructured materials are relatively more disordered and inherently contain a certain amount of excess volume in the form of vacancies and vacancy clusters [50–54]. According to elasticity theory [55, 56], these excess volumes may create stress field which exerts lattice strain in nanocrystalline materials. Furthermore, for smaller crystallites, the internal pressure exerted by the surface tension on the nano materials may produce a stress field resulting lattice strain. However, as the crystallite size increases, the grain boundary stress field becomes weak causing decrease

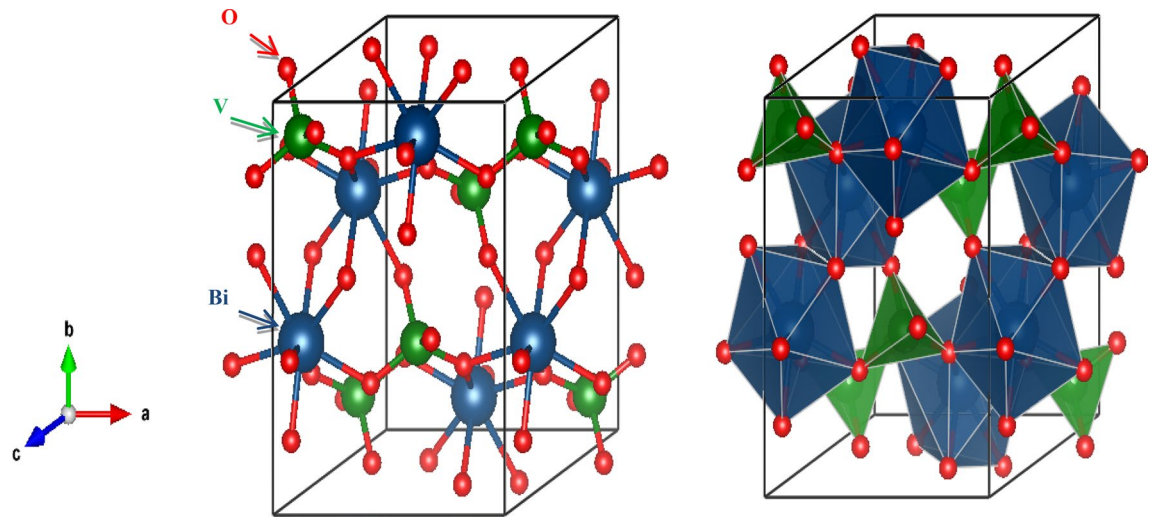

Fig. 2 The crystal structure of monoclinic clinobisvanite $BiVO_4$ and corresponding polyhedron structure—BiO_8 dodecahedron in blue and VO_4 teterahedron in green

Table 2 Crystallite size and lattice strain with respect to synthesis temperature

Synthesis temperature (°C)	Crystallite size (nm)	Lattice strain (%)
500	51.9	0.260
550	77.6	0.189
600	86.5	0.175
650	151.0	0.117
700	153.8	0.116

of lattice strain [46, 57]. So, the excess volume near grain boundaries as well as the crystallite interface both highly contribute to stress field and could be the plausible sources of internal strain with decreasing crystallite size [46, 48].

FTIR spectra (Fig. 3) analyzed at room temperature demonstrate strong and broad IR band at 718 cm^{-1} with shoulder at 802 cm^{-1} which is a characteristic of m-$BiVO_4$. In addition, a small IR band is observed at 466 cm^{-1}. According to literature, the strong IR band at 718 cm^{-1} is due to anti-symmetric stretching vibration from VO_4 and the weak IR band at 466 cm^{-1} results from absorption of Bi-O bond [58]. Powder synthesized at 500 °C shows V–O stretching of V_2O_5 (1009 cm^{-1}) and presence of V_2O_5 at low temperature (500 °C) is also confirmed by XRD analysis [59].

The diffuse reflectance of the $BiVO_4$ samples was measured in the wavelength range of 200–800 nm from which absorbance versus wavelength plot was constructed (Fig. 4a). The diffuse reflectance data were converted to Kubelka–Munk function given by $F(R)=(1-R)^2/2R$ (where R is the diffuse reflectance value) to construct the $[F(R)\,h\upsilon]^{1/n}$ vs. $h\upsilon$ (photon energy) plots for the fabricated samples

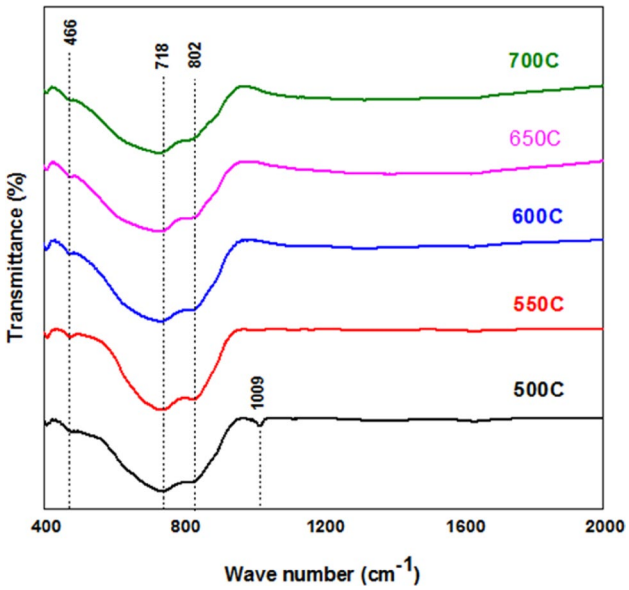

Fig. 3 FTIR spectra of m-$BiVO_4$ powders obtained from different synthesis temperature

(Fig. 4b) [60]. The electronic structure as well as sharp fall of the graph of m-$BiVO_4$ indicate that it possesses features of direct band gap semiconductor and we used n = 1/2 for direct electronic transition. Here, the intersection of the tangent line with $[h\upsilon\,F(R)]^2=0$ represents the optical band gap energy, e.g. The band gap energies obtained for the samples are quite consistent with the reported band gap values of the monoclinic $BiVO_4$. From the plot, red shift of band gap is observed (2.49–2.37 eV) as the fabrication temperature rises (500–700 °C). The absorption edge of the prepared m-$BiVO_4$ also reveals red shift and their corresponding

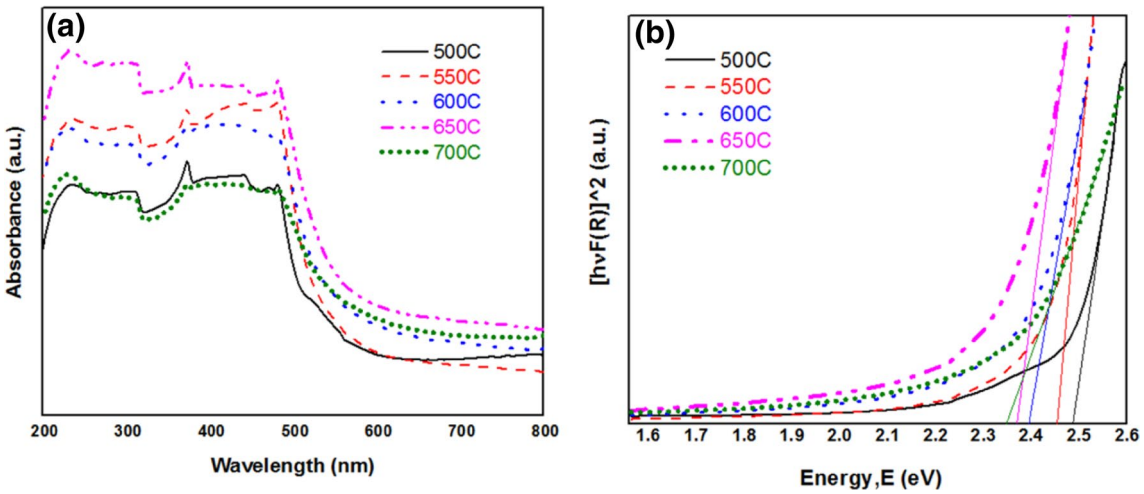

Fig. 4 **a** UV–Vis absorption spectra derived from diffuse reflectance spectra of $BiVO_4$ particles synthesized at different temperatures, **b** $[h\upsilon F(R)]^2$ versus photon energy plots to calculate band gap energy of the corresponding samples

Table 3 Absorption edge and band gap with respect to synthesis temperature

Synthesis temperature (°C)	Absorption edge (nm)	Band gap (eV)
500	499.25	2.49
550	507.40	2.45
600	517.97	2.40
650	522.32	2.38
700	526.75	2.36

values (absorption edge and band gap) with respect to temperature are summarized in Table 3. When crystallite size decreases to nanoscale the number of atoms becomes smaller in a crystal which results less overlapping of energy levels and width of each band (valence and conduction) starts to narrow. Consequently, band gap increases as crystallite size decreases. Furthermore, at higher calcination temperature all active electronic regions at the surface of the particles are subdued along with their size increase and so absorption spectra show this phenomenon [58].

The FESEM micrographs shown in Fig. 5a–e, reveal that the microstructures contain agglomerated particles. The agglomeration occurs mainly due to the effects of electrostatic forces at the interfaces and Van der Waals interactions [3]. The particles are nearly spherical in shape with non-uniform size distribution when synthesized up to 550 °C. However, at higher temperatures above 550 °C, the $BiVO_4$ samples show particles with irregular shape morphology. It is observed that particle size increases with increasing synthesis temperature (Fig. 5). Figure 6a–e show EDS spectra of the particles and Table 4 gives the elemental compositions. The characteristic X-ray radiation of each element has different energy values: bismuth $M_\alpha = 2.419$ keV, vanadium $K_\alpha = 4.949$ keV and oxygen $K_\alpha = 0.525$ keV. It is evident that no pollutant is present in the prepared particles and atomic ratio of Bi, V and O is nearly 1:1:4.

4 Conclusion

In this research, a simple method of producing pure m-$BiVO_4$ nanoparticles has been presented. XRD patterns confirm formation of highly crystalline m-$BiVO_4$. The yield of m-$BiVO_4$ increases as reaction temperature rises and single phase m-$BiVO_4$ is found in all samples calcined above 550 °C. Besides, it is evident that crystallite size increases (employing Scherrer formula) and red shift of band gap occurs (2.49–2.37 eV), in the synthesized particles with respect to temperature rise (500–700 °C). The vibrational properties measured by FTIR spectra also show conformity with m-$BiVO_4$. FESEM micrographs reveal that at lower temperatures (500 °C and 550 °C) the particles are nearly spherical, whereas they are irregular in shape at higher temperatures (600 °C, 650 °C and 700 °C). The above study on structural, optical and morphological properties of the prepared m-$BiVO_4$ particles suggests them as promising photocatalyst.

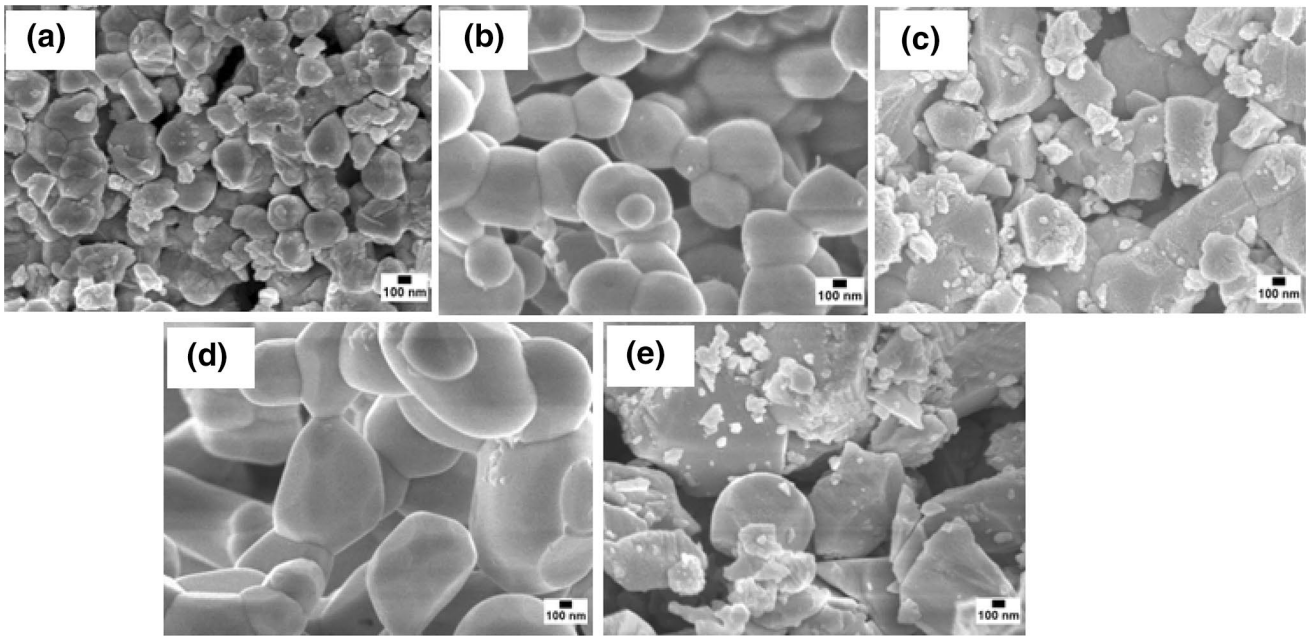

Fig. 5 FESEM micrographs of $BiVO_4$ particles synthesized at **a** 500 °C, **b** 550 °C, **c** 600 °C, **d** 650 °C, and **e** 700 °C, at magnification ×30,000

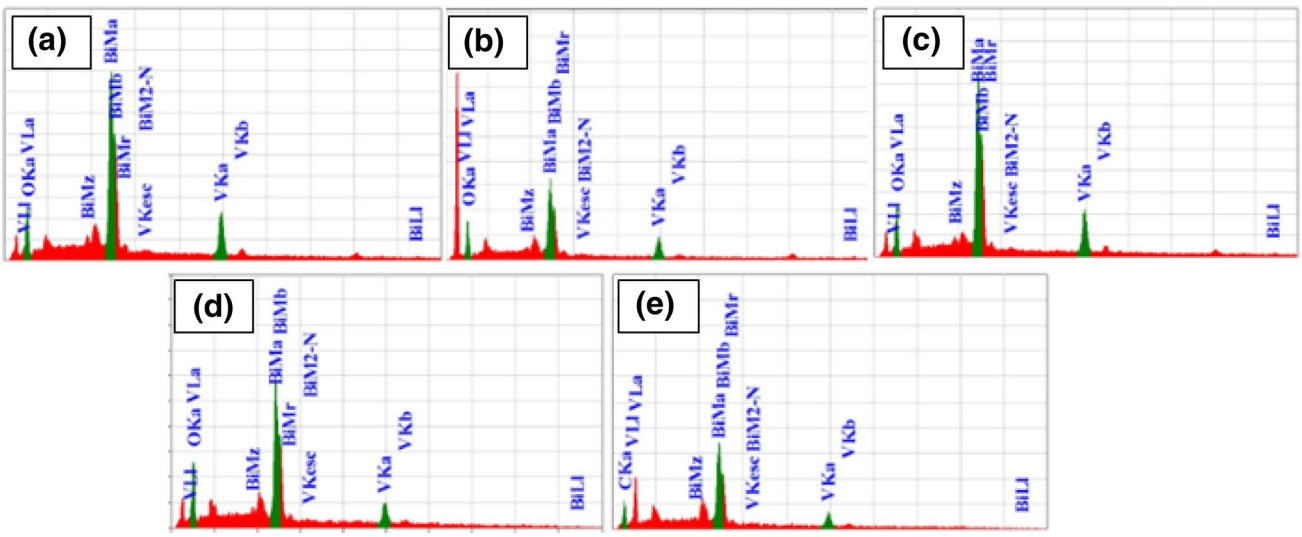

Fig. 6 EDS spectra recorded from prepared powders: **a** $BiVO_4$ 500 °C, **b** $BiVO_4$ 550 °C, **c** $BiVO_4$ 600 °C, **d** $BiVO_4$ 650 °C and **e** $BiVO_4$ 700 °C

Table 4 Element concentrations calculated from EDS analysis of $BiVO_4$ nanoparticles

Temperature	Elements		
	Bi	V	O
500 °C			
Mass%	64.84	15.14	20.02
Atom%	16.83	16	67.17
550 °C			
Mass%	64.54	15.36	20.1
Atom%	16.67	16.33	67
600 °C			
Mass%	64.9	15.01	20.09
Atom%	16.83	15.83	67.33
650 °C			
Mass%	64.71	15.41	19.88
Atom%	16.67	16.33	67
700 °C			
Mass%	64.5	15.38	20.12
Atom%	16.67	16.33	67

Acknowledgements The authors would like to thank Department of Glass and Ceramic Engineering, Bangladesh University of Engineering and Technology (BUET) for providing assistance regarding characterization and preparation of the specimen.

Compliance with Ethical Standards

Conflict of interest There is no conflict of interest in writing and publishing the manuscript.

References

1. D.W. Chen, A.K. Ray, Appl. Catal. B: Environ. **23**, 143–157 (1999)
2. H. Zhou, D.W. Smith, J. Environ. Eng. Sci **1**, 247–264 (2002)
3. V. Rajalingam, Synthesis and characterization of $BiVO_4$ nanostructured materials: application to photocatalysis. Dissertation, Universit´e du Maine (2014)
4. F.M. Toma, J.K. Cooper, V. Kunzelmann, M.T. McDowell, J. Yu, D.M. Larson, N.J. Borys, C. Abelyan, J.W. Beeman, K. Man, J. Yang, L. Chen, M.R. Shaner, J. Spurgeon, F.A. Houle, K.A. Persson, I.D. Sharp, Nat. Commun. **7**, 12012 (2016)
5. K. Ordon, Functionalized semiconducting oxides based on bismuth vanadate with anchored organic dye molecules for photoactive applications. Dissertation, Université du Maine (2018)
6. M.J. Madiabu, J. Gunlazuardi, AIP Conf. Proc. **2023**, 020079 (2018)
7. A. Fernandez, G. Lassaletta, V.M. Jimenez, A. Justo, A.R. Gonzalez Elipe, J.M. Herrmann, H. Tahiri, Y. Aitichou, Appl. Catal. B: Environ. **7**, 49–63 (1995)
8. C. Minero, E. Pelizzetti, P. Pichat, M. Sega, M. Vincenti, Environ. Sci. Technol. **29**, 2226–2234 (1995)
9. S.S. Wu, H.Q. Cao, S.F. Yin, X.W. Liu, X.R. Zhang, J. Phys. Chem. C **113**, 17893–17898 (2009)
10. L. Gao, L.Q. Jiang, Mater. Chem. Phys. **91**, 313–316 (2005)
11. M.A. Gondal, K. Hayat, M.M. Khaled, S. Ahmed, A.M. Shemsi, Appl. Catal. A **393**, 122–129 (2011)
12. W.Z. Wang, H.L. Xu, W. Zhu, J. Phys. Chem. B **110**, 13829–13834 (2006)
13. K. Rajeshwar, S. Somasundaram, C.R.N. Chenthamarakshan, N.R. de Tacconi, Int. J. Hydrog. Energy **32**, 4661–4669 (2007)
14. M.A.A. Mamun, A.F.M.M. Hossain, M. Hasan, M.M. Rahman, Hydrothermal Synthesis and Characterization of Bismuth Vanadate Photocatalyst, in *Proceedings of the 1st International Conference on Engineering Materials and Metallurgical Engineering*, Bangladesh Council of Scientific and Industrial Research, Dhaka, 22–24 December 2016
15. H. Cai, L. Cheng, F. Xu, H. Wang, W. Xu, F. Li, R. Soc, Open Sci. **5**, 180752 (2018)
16. A. Fujishima, K. Honda, Nature **238**(5358), 37–38 (1972)
17. A. Kudo, K. Ueda, H. Kato, I. Mikami, Cat. Let. **53**, 229 (1998)
18. P.H. Le, N.T. Kien, C.N. Van, *Recent Advances in $BiVO_4$- and Bi_2Te_3-Based Materials for High Efficiency-Energy Applications* (Intech Open, London, 2018)
19. S. Dolic, D. Jovanovic, L. Zur, M. Cincović, M. Ferrari, M. Dramićanin, Synthesis, multifunctional properties and applications of bivo4 nanoparticles (Conference Presentation), in *Proceeding of SPIE 10683, Fiber Lasers and Glass Photonics: Materials through Applications*, 106831G (23 May 2018)
20. F. Rullens, A. Laschewsky, M. Devillers, Chem. Mater. **18**, 771 (2006)
21. M.F. Rahman, M.S. Haque, M.H. Rizvi, M.A. Matin, M.A. Hakim, M.F. Islam, in *Abstracts of the International Conference on Nanotechnology and Condensed Matter Physics*, Bangladesh University of Engineering and Technology, Dhaka, 11–12 January 2018
22. M. Noor, M.A.A. Mamun, M.A. Matin, M.F. Islam, S. Haque, F. Rahman, M.N. Hossain, M.A. Hakim, Effect of pH Variation on Structural, Optical and Shape Morphology of $BiVO_4$ Photocatalysts, in *10th International Conference on Electrical and Computer Engineering* (IEEE, Dhaka, 20–22 December, 2018). https://doi.org/10.1109/icece.2018.8636721
23. H. Zhao, F. Tian, R. Wang, R. Chen, Rev. Adv. Sci. Eng. **3**, 3–27 (2014)
24. Z. Wang, W. Luo, S. Yan, J. Feng, Z. Zhao, Y. Zhu, Z. Li, Z. Zou, Cryst. Eng. Commun. **13**, 6674–6679 (2011)
25. P. Madhusudan, J. Yu, W. Wang, B. Cheng, G. Liu, Dal. Trans. **41**, 14345–14353 (2012)
26. A. Walsh, Y. Yan, M.N. Huda, M.M. Al-Jassim, S.H. Wei, Chem. Mater. **21**, 3 (2009)
27. Z. Zhao, Z. Li, Z. Zou, Phys. Chem. Chem. Phys. **13**, 4746–4753 (2011)
28. U.M.G. Perez, S.S. Guzman, A.M. de la Cruz, J. Peral, Int. J. Electrochem. Sci. **7**, 9622–9632 (2012)
29. D.P. Dubal, K. Jayaramulu, R. Zboril, R.A. Fischer, P.G. Romero, J. Mater. Chem. A **6**, 6096 (2018)
30. T.L. Kim, M.J. Choi, H.W. Jang, Boosting interfacial charge transfer for efficient water-splitting photoelectrodes: progress in bismuth vanadate photoanodes using various strategies. MRS Commun. **8**, 3 (2018)
31. M. Guo, Q. He, W. Wang, J. Wu, W. Wang, J. Wuhan Univ. Technol.-Mater. Sci. Edit. **31**, 791 (2016). https://doi.org/10.1007/s11595-016-1447-z
32. M. Peng, J. Shi, Z. Wang, L. Li, Penglong CHEN Improvement of synthesis experiment of bismuth vanadate pigment by pH optimization. Univ. Chem. **33**(8), 26–31 (2018)
33. M.V. Malashchonak, E.A. Streltsov, D.A. Kuliomin, A.I. Kulak, A.V. Mazanik, Monoclinic bismuth vanadate band gap determination by photoelectrochemical spectroscopy. Mater. Chem. Phys. (2017). https://doi.org/10.1016/j.matchemphys.2017.08.053
34. A.N. Zulkifili, A. Fujiki, S. Kimijima, Appl. Sci. **8**, 216 (2018)

35. S.D. Dolića, D.J. Jovanovića, K. Smitsb, B. Babićc, M.M. Cincovića, S. Porobića, M.D. Dramićanina, Ceram. Int. **44**, 17953–17961 (2018)
36. V. Sivakumar, R. Suresh, K. Giribabu, V. Narayanan, Cogent. Chem. **1**, 1074647 (2015)
37. A. Kudo, K. Omori, H. Kato, J. Am. Chem. Soc. **121**(49), 11459–11467 (1999)
38. S. Khademinia, M. Behzad, H.S. Jahromi, RSC Adv. **5**, 24313–24318 (2015)
39. J. Yu, Y. Zhang, A. Kudo, J. Solid State Chem. **182**, 223–228 (2009)
40. S.M. Thalluri, C.M. Suarez, M. Hussain, S. Hernandez, A. Virga, G. Saracco, N. Russo, Evaluation of the parameters affecting the visible-light-induced photocatalytic activity of monoclinic $BiVO_4$ for water oxidation. Ind. Eng. Chem. Res. **52**, 17414–17418 (2013). https://doi.org/10.1021/ie402930x
41. Y.K. Kho, W.Y. Teoh, A. Iwase, L. Maedler, A. Kudo, R. Amarl, ACS. Appl. Mater. Interfaces **3**(6), 1997–2004 (2011)
42. C. Ravidhas, A.J. Josephine, P. Sudhagar, A. Devadoss, C. Terashima, K. Nakata, A. Fujishima, A.M.E. Raj, C. Sanjeeviraja, Mater. Sci. Semicond. Process. **30**, 343–351 (2015)
43. Q. Jia, K. Iwashina, A. Kudo, Proc. Natl. Acad. Sci. **109**, 11564–11569 (2012)
44. K. Rajeshwar, N.R. Tacconi, Chem. Soc. Rev. **38**, 1984–1998 (2009)
45. S. Obregón, A. Caballero, G. Colón, Appl. Catal. B: Environ. **117–118**, 59–66 (2012)
46. P.M. Shafi, A.C. Bose, AIP Adv. **5**, 057137 (2015)
47. W. Qin, J.A. Szpunar, Phil. Mag. Lett. **85**, 653 (2005)
48. K. Reimann, R. Wurschum, J. Appl. Phys. **81**, 7186 (1997)
49. T.R. Malow, C.C. Koch, Acta Mater. **45**, 2177 (1997)
50. W. Qin, T. Nagase, Y. Umakoshi, J.A. Szpunar, Philos. Mag. Lett. **88**(3), 169–179 (2008)
51. D.H. Ping, D.X. Li, H.Q. Ye, J. Mater. Sci. Lett. **14**, 1536 (1995)
52. K. Lu, Mater. Sci. Eng. R. **16**, 161 (1996)
53. K. Lu, R. Lück, B. Predel, Mater. Sci. Eng. A. **179–180**, 536 (1994)
54. P.P. Chattopadhyay, P.M.G. Nambissan, S.K. Pabi et al., Phys. Rev. B. **63**, 054107 (2001)
55. W. Qin, J.A. Szpunar, Philos. Mag. Lett. **85**(12), 649–656 (2005)
56. J.W. Christian, *The Theory of Transformations in Metals and Alloys, Part 1* (Pergamon Press, Oxford, 2002), pp. 202–203
57. M. Dapiaggi, C.A. Geiger, G. Artioli, Am. Miner. **90**, 506 (2005)
58. R. Venkatesan, S. Velumani, A. Kassiba, Mat. Chem. Phys. **135**, 842–848 (2012)
59. H.D. Telpande, D.V. Parwate, J. Appl. Chem. **8**(5), 28–37 (2015)
60. P. Kubelka, F. Munk, EinBeitrag ZurOptik Der Farbanstriche. Zeitschriftfür Technische Physik. **12**, 593–601 (1931)